

The use of high resolution magnetic resonance on 3.0-T system in solid/multicystic ameloblastoma surgical planning

Case report



Ann. Ital. Chir., 2014 85: 219-224
pii: S0003469X14020557

Michele Cassetta*, Nicola Pranno*, Stefano Di Carlo*, Valentina Sorrentino**, Andrea Stagnitti**, Giorgio Pompa*

*Department of Oral and Maxillofacial Sciences, "Sapienza" University of Rome, Rome, Italy.

**Department of Radiological Sciences, Oncology and Pathology "Sapienza" University of Rome, Rome, Italy

The use of high resolution magnetic resonance on 3.0-T system in solid/multicystic ameloblastoma surgical planning. Case report.

OBJECTIVES: *The solid/multicystic ameloblastoma is a slowly growing, locally invasive epithelial odontogenic tumour. In 80% of cases this lesion occurs in the mandible, mainly in the posterior region, and it is characterized by the involvement of the inferior alveolar nerve. A panoramic radiograph of a 43-year-old man with chronic deep pain in the posterior area of the mandible showed a multilocular radiolucent lesion with scalloped borders in the left mandibular ramus. After the execution of a computed tomography of the jaws, to accurately determine the limits of the lesion and the relationship with the the inferior alveolar nerve, the magnetic resonance imaging was used.*

METHODS: *The spatial relationship between the lesion and the inferior alveolar nerve was defined comparing different imaging methods: panoramic radiography, computed tomography and magnetic resonance imaging. T1-weighted fast spoiled gradient-recalled echo, T1-weighted fast imaging employing steady-state acquisition, T2-weighted interactive decomposition of water and fat with echo asymmetry least-squares estimation and Diffusion weighted imaging acquisition sequences were used on a 3.0 T unit.*

RESULTS: *Regarding the inferior alveolar nerve course and its spatial relationship with the mandibular lesion, magnetic resonance imaging provided more detailed spatial and structural information than other imaging methods.*

CONCLUSION: *The described acquisition sequences allowed us to highlight the diagnostic efficacy of the magnetic resonance in the morpho-structural characterization of a maxillofacial lesion and showed the importance of this imaging method as an additional technique to the computerized tomography in the maxillofacial surgical planning, resulting in a risk reduction of the inferior alveolar nerve surgical injury.*

KEY WORDS: Ameloblastoma, Mandibular Nerve, Magnetic Resonance Imaging, Tomography X-Ray Computed.

Introduction

The solid/multicystic ameloblastoma is the second most common odontogenic tumour; it is mostly diagnosed

between 30 and 60 years of age, rarely below the age of 20 years. This tumour is characterized by a low speed expansion and it is frequently associated to a local invasion of the contiguous epithelial areas¹. The pre-operative evaluation in oral maxillofacial surgery is currently performed by several imaging methods. One of the principal difficulties in the surgical planning is to define the anatomic relation among the lesion and peripheral nerves. The evaluation of the spatial relationship between the inferior alveolar nerve (IAN) course and a mandibular lesion is important to avoid injuries of this anatomic structure²⁻¹³.

Pervenuto in Redazione Settembre 2012. Accettato per la pubblicazione Marzo 2013

Correspondence to: Michele Cassetta DDS, PhD, Assistant Professor, Department of Oral and Maxillofacial Sciences, "Sapienza" University of Rome, Italy, School of Dentistry (e-mail: michele.cassetta@uniroma1.it)

Both panoramic radiography (OPT) and computerized tomography (CT) can be used to detect the bone structures. However, the efficacy of these imaging methods in the IAN course detection is lower than magnetic resonance imaging (MRI). In fact, while CT and OPT can clearly depict the bone structure of the mandibular canal, MRI allows a significant appreciation of its contents¹⁴⁻¹⁷.

In the present case report, the use of the MRI was used to evaluate the limits and structural characterization of a severe case of solid/multicystic ameloblastoma and to determine the relationship with the the inferior alveolar nerve¹⁸. Moreover, a comparative analysis among OPT, CT and MRI approaches was performed.

Case Report

A 48-year-old man with deep pain on the left side of the mandible that began two months before. The clinical examination did not show oral inflammation of the mucosa, nor bone-like swelling in the corresponding area of the mandible; the only clinical feature observed was a suppurating fluid leakage from the gingival margin of the second molar, determining foetor ex-ore.

OPT revealed a multiple-locus radiolucency presenting scalloped and well defined margins, interesting the whole left mandibular ramus. The lesion determined the resorption of the anterior margin of the mandible (Fig. 1). CT showed a lesion with a characteristic "soap bubble" shape (41 mm x 14 mm) (Fig. 2: a-c). Axial CT imaging highlighted a wide lesion from the upper part of the mandibular ramus (under the mandibular notch) to the alveolar bone distally to the second mandibular molar; no basal bone involvement was detected (Fig. 2a). Sagittal CT imaging revealed involvement of the anterior margin of the ramus; the mandibular angle was not interested (Fig. 2b). Moreover, the lesion induced the resorption of the mandibular canal roof (Fig. 2b). Coronal CT imaging showed erosion of both medial and lateral cortical bone of the left mandibular ramus (Fig. 2c).

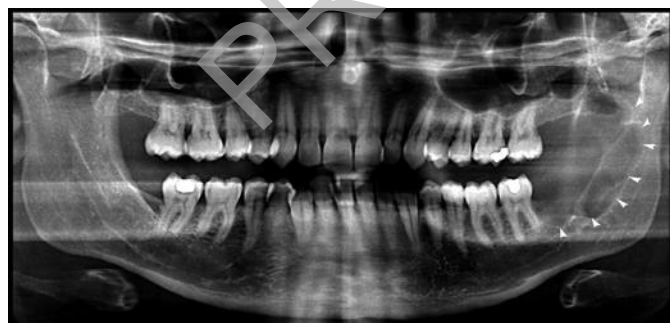


Fig. 1: Panoramic radiography (OPT) of a multilocular radiolucent lesion that involves the left mandibular ramus. The white arrows highlight the posterior margins of the lesion.

MRI was performed on a 3.0-T system (Discovery MR750, GE Healthcare, Milwaukee-WIS, USA). Unenhanced T1-weighted (Figs 2: d-f) and T2-weighted sequences were initially acquired with and without fat suppression; this allowed to detect the morphologic features of the lesion and its anatomic relation with the IAN. Contrast-enhanced MRI (CE-MRI) with gadoteric acid (DOTAREM, 12 ml) was performed to evaluate possible soft tissue invasion and to investigate the benign nature of the lesion.

Since extensive resections provide discomfort (i.e. masticatory dysfunction, facial deformity or abnormal mandibular movements) and seriously compromise the patient's quality of life, according to the current trend of the scientific community a less invasive surgery treatment was initially performed².

A conservative approach and evaluation of clinical results was used.

The lesion was treated conservatively with cystectomy and curettage of peripheral bone.

The surgery was performed under general anesthesia. The surgical incision allowed to expose the whole left mandibular ramus. Medial and lateral soft tissues were elevated and immobilized using a suture. The point of communication of the lesion with the oral cavity has been used as a starting point to broaden the access to the bone lesion. The size of bone access were extended to the 2/3 of the lesion to allow its entire excision. The lesion was detached from the bone structures using a periosteals upholstered with gauze in order to limit the risk of tearing the neoformation. After detaching the 2/3 of neoplasia, the remnant 1/3 was excised using a tissue forcep. The pulling action of tissue forcep was added to the action of detachment of the periosteal. The mass was excised completely and entirely and this was very important to reduce the risk of recurrence. The revision of the residual cavity was performed and the inferior alveolar nerve was preserved. Since the cavity had containment capacity it was not necessary to perform any kind of restorative treatment. The surgery was completed with suture.

The integrity of the inferior alveolar nerve was preserved, and there were no post-operative neurological disorders.

The X-ray follow-up at 12 months showed signs of healing with re-mineralization of the residual bone cavity.

Histological findings showed a tumour mass characterized by follicular growth pattern with fibrous stroma; isolated ghost cells and infiltrating inflammatory cells were found; the follicular nests were composed by palisaded columnar cells surrounding arranged stellate reticulum-like cells. Plexiform pattern was detected exclusively in isolated regions of the tumor mass.

The lesion was finally diagnosed as solid/multicystic type ameloblastoma composed by dominant follicular growth pattern, according to the 2005 WHO Histological classification of odontogenic tumours.

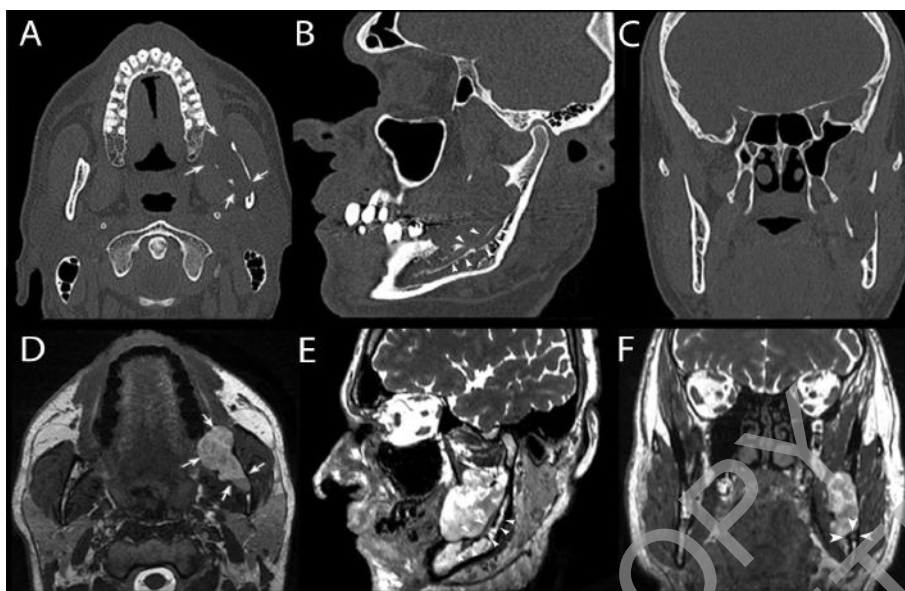


Fig. 2: A) Axial CT highlights the left mandibular ramus involvement with erosion of both medial and lateral cortical bone; B) Sagittal CT shows the erosion of the anterior margin of the mandible and resorption of the mandibular canal roof; C) Coronal CT confirms medial and lateral cortical bone erosion in the left mandibular ramus. The relationship between the mandibular canal and the inferior margin of the lesion is not detectable; D) T1-weighted fast imaging employing steady-state acquisition (FIESTA), axial image: the anatomical limits of the lesion are more clearly detectable; E) T1-weighted fast imaging employing steady-state acquisition (FIESTA), sagittal image: the IAN course and the lesion can be clearly revealed (the arrows indicate the IAN course); F) T1-weighted fast imaging employing steady-state acquisition (FIESTA), coronal image: the relationship between the IAN (arrows) and the inferior margin of the lesion can be well evaluated. The white arrows indicate the IAN and the lesion.

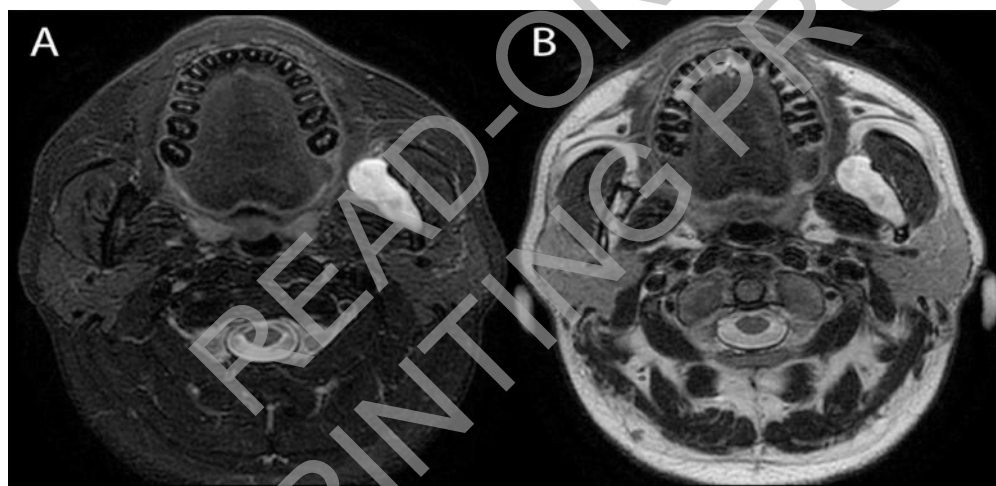


Fig. 3: T2-weighted axial images acquired with a fast spin echo interactive decomposition of water and fat with echo asymmetry and leastsquares estimation (FSE IDEAL). Water A) and Fat B) (T2 FSE-IDEAL) show an heterogeneous pattern within the tumour mass.

Discussion

Since CT imaging can provide precise information about the bone resorption, in case of mandibular lesions this imaging technique is currently used in oral and maxillo-facial surgery to perform a detailed evaluation of the bone structures.

However, in previous studies CT imaging has often provided unclear depiction of the mandibular canal contents and low definition of thin peripheral nerves, particularly for the incisal nerve, one of the terminal branches of the

IAN.²⁻¹³ In contrast, the present MRI protocol provided high resolution images of these anatomic structures and together with the CT imaging was decisive for the surgical planning and for the risk reduction of IAN damage. Since the maxillofacial area is composed by a high percentage of fat and fluid, the study of this region could not be performed by means of routine conventional techniques of MRI. Consequently, our protocol was carried out using the following sequences:

1) T2-weighted axial images acquired with a fast spin echo interactive decomposition of water and fat with

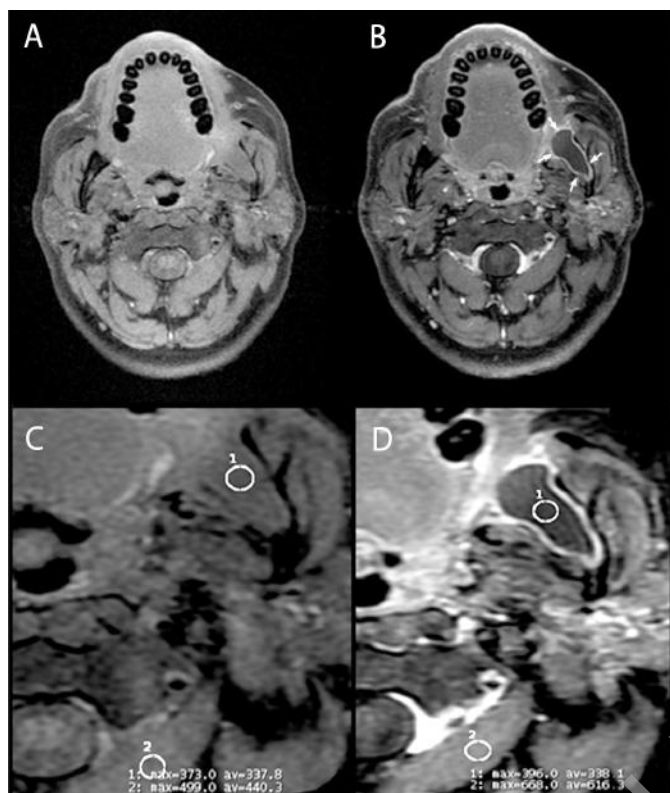


Fig. 4: T1-weighted axial images fat-saturated fast spin echo (Ax T1 Fs FSE); A) pre-contrast administration (Ax T1 Fs FSE pre-CE); B) post-contrast administration (Ax T1 Fs FSE post-CE). The post-CE acquisition shows that the contrast is confined to the margin of the lesion, characteristic image of the benign tumour with the presence of a capsule. Two ROIs corresponding to the lesion (1) and to the muscular tissue (2) were determined in the pre C) and post-contrast administration D) sequences. A significant different gradient between the two sequences was detected only in the muscular tissue. Consequently no mass enhancement was observed.

echo asymmetry and least-squares estimation (FSE IDEAL) using a repetition time (TR) of 3038 ms, echo time (TE) of 124 ms, field of view (FOV) of 24 x 24 cm, slice-thickness (SL) of 4 mm, and number of excitations (NEX) of 3 (Fig. 3).

The IDEAL sequence allowed to acquire 3 images with different phase shifts between water (Fig. 3a) and fat (Fig. 3b) saturation thus leading to the possibility to distinguish water and fat images and the field map.

In order to obtain this separation, iterative fat-water decomposition algorithm and a 3-echo data acquisition, with the center echo shifted relative to the SE point, were combined. This sequence allows to depict the component (solid or liquid) of the lesion.

In the Water: (T2 FSE-IDEAL) the lesion appeared as a high signal intensity region (Fig. 3a), while it was characterized by intermedial-low intensity in the Fat: (T2 FSE-IDEAL) (Fig. 3b). Both the sequences unveiled an heterogeneous pattern within the tumour mass, commonly observed in ameloblastoma (Fig. 3).

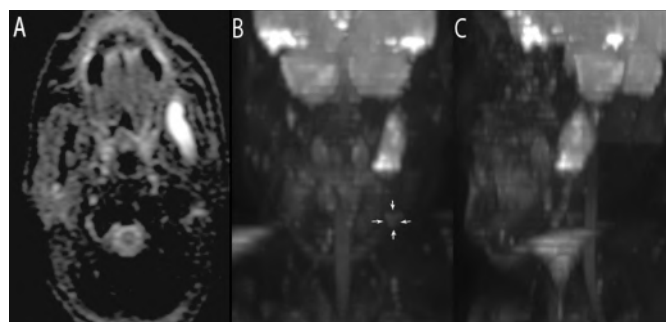


Fig. 5: Diffusion weighted imaging acquisition (DWI b=800): A) Axial diffusion-weighted MR image at $b = 800 \text{ s/mm}^2$ shows a high signal intensity of the lesion; B, C) High resolution 3D Volume Rendering 3DVR-MRI shows enlarged nodes, ipsilateral to the lesion, in the upper part of the neck which exhibit low signal intensity. The white arrows indicate an enlarged node.

2) T1-weighted axial images fat-saturated fast spin echo pre-contrast administration (Ax T1 Fs FSE pre-CE) (Fig. 4a) and post-contrast administration (Ax T1 Fs FSE post-CE) (Figure 4b) using a repetition time (TR) of 418 ms, echo time (TE) of 8 ms, field of view (FOV) of 25 x 25 cm, slice-thickness (SL) of 4 mm, and number of excitations (NEX) of 2 were acquired to evaluate the potential enhancement of the mass.

The contrast index (CI) pre-figure 4 c) and post-contrast (Figure 4d) administration was calculated using one region of interest (ROI) in the centre of the tumour mass (a ROI in the muscular tissue was used as a control-image). No significant differences were observed in the CI between the two ROIs. Contrast-enhanced MRI revealed an encapsulated lesion and highlighted well defined margins; this finding allowed us to assign the diagnosis of a benign tumour, such as ameloblastoma.

3) Diffusion weighted imaging (DWI b=800) using a repetition time (TR) of 4375 ms, echo time (TE) of 72 ms, field of view (FOV) of 23 x 23 cm, slice-thickness (SL) of 5mm, bandwidth (b) of 800 s/mm^2 and number of excitations (NEX) of 1 (Fig. 5).

DWI evaluates intercellular water motion: every change in the water protons movements induces a variation of signal intensity in this sequence. Diffusion-weighted imaging is currently used to improve the diagnostic accuracy in the differential diagnosis between benign and malignant nodes. Metastatic nodes are characterized by reduction of diffusivity, which is associated with a hypercellularity, to an increased nuclear-to-cytoplasmic ratio and a perfusion¹⁹⁻²⁵. This decrement in diffusion is represented as an area of hyperintensity on diffusion images; adversely, inflammatory nodes appear hypointense. The DWI sequence showed a benign latero-cervical lymphadenopathy, ipsilateral to the lesion, in the upper part of the neck. No malignant lymph nodes were observed. (Fig. 5).

The presence of intermedial signal intensity on T1WI, bright signal intensity on T2WI and no enhancement on CE-T1WI suggested a prevalent multicystic compo-

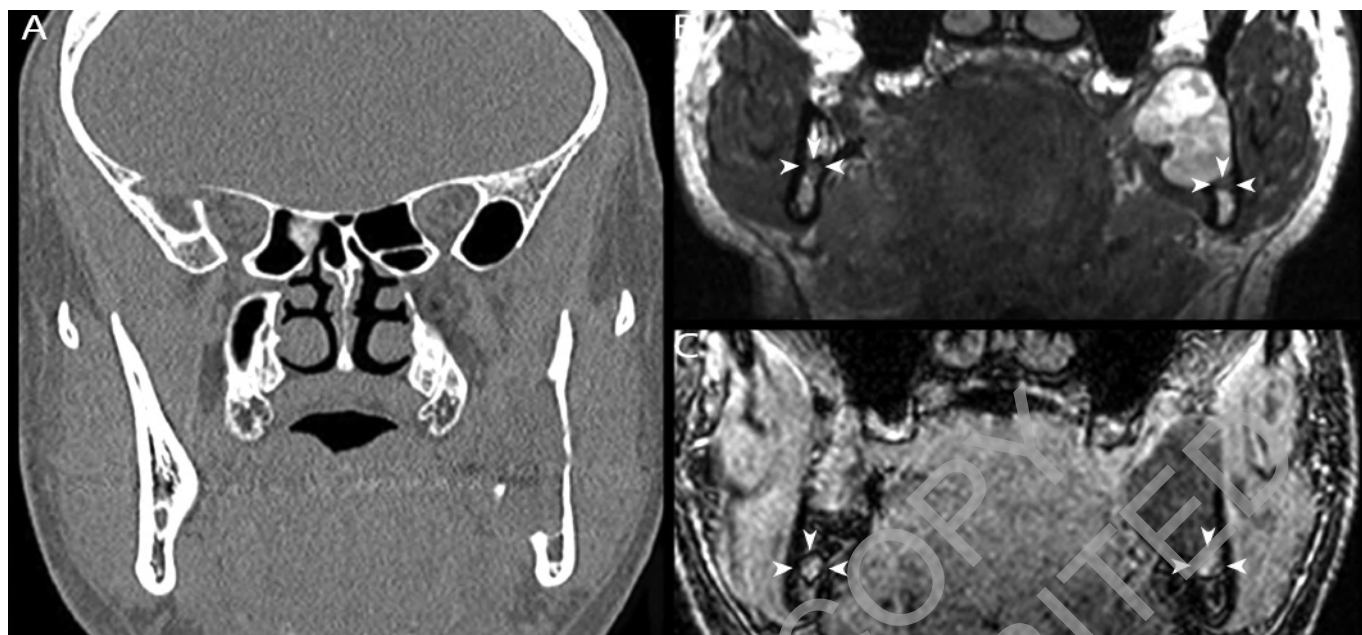


Fig. 6: In the Coronal CT images A) the relationship between the lesion and the mandibular canal is not detectable; in the coronal T1-weighted fast imaging employing steady-state acquisition (FIESTA) B) and in the coronal T1-weighted fast spoiled gradient-recalled echo (fast SPGR) C) the relationship between the lesion and IAN (white arrows) is clearly detectable.

ment of the ameloblastoma. A minor solid pattern, characterized by intermedial signal intensity in T1WI, high signal intensity in T2WI and good enhancement, was observed^{21,22}.

4) T1-weighted fast imaging employing steady-state acquisition (FIESTA) using a repetition time (TR) of 4.6 ms, echo time (TE) of 2.2 ms, field of view (FOV) of 24 x 24 cm, slice-thickness (SL) of 0.6 mm and number of excitations (NEX) of 1 and T1-weighted fast spoiled gradient-recalled echo (fast SPGR) using a repetition time (TR) of 7.8 ms, echo time (TE) of 3.2 ms, field of view (FOV) of 23.5 x 23.5 cm, slice-thickness (SL) of 0.6 mm and number of excitations (NEX) of 2 (Figs. 6 b,c).

These sequences provided a precise estimation of the distance between the lesion and the IAN supplementing clear anatomical visualization (Figs. 6 b,c). This allowed us to visualize the contact between the IAN and the lesion located in the lower part of the mandibular ramus due to erosion of the mandibular canal (Figs. 6 b,c), which could not be clearly observed with CT imaging (Fig 6a).

MRI has been infrequently used for the maxillo-facial region because the acquisition of the sequences can be invalidated by motion of the body, respiration, air in the oral cavity and nasal cells, implants and metal materials^{3,27}. However utilization of this diagnostic method provided a careful morpho-structural characterization and evaluation of spatial relationship between IAN and a mandibular lesion avoiding damages of this anatomic structure.

In conclusion, in order to perform a correct oral and maxillofacial surgical planning, CT imaging remains a

fundamental technique to obtain precise information about the tumor mass extension inside the bony structure, but the capability to acquire more information without exposing the patient to x-rays makes the MRI a supplementary method which was proved to be crucial in maxillo-facial surgical planning in order to reduce substantially the risk of IAN damage.

Riassunto

OBIETTIVI: L'ameloblastoma nella variante solida / multicistico è caratterizzato da una lenta crescita, localmente invasiva all'interno del tessuto osseo. Nel 80% dei casi questa lesione insorge nella mandibola, soprattutto nella regione posteriore, con interessamento del nervo alveolare inferiore. Una Rx ortopantomica di un uomo di 43 anni, con dolore cronico profondo nella zona posteriore della mandibola, ha evidenziato una lesione radiotrasparente multiloculare con bordi festonati nel ramo mandibolare sinistro.

In aggiunta all'esecuzione di una tomografia computerizzata della mandibola sono state utilizzate delle particolari sequenze di risonanza magnetica per determinare con precisione i limiti della lesione ed il rapporto che essa contrae con il nervo alveolare inferiore, al fine di valutare il ruolo che questa tecnica di imaging può avere nella fase della programmazione chirurgica.

METODI: Il rapporto spaziale tra la lesione e il nervo alveolare inferiore è stato analizzato confrontando i diversi metodi di immagine: RX ortopantomica, tomografia

computerizzata e risonanza magnetica con unità 3.0-T. Le sequenze utilizzate nell'esame di risonanza magnetica sono state: T1-weighted fast spoiled gradient-recalled echo, T1-weighted fast imaging employing steady-state acquisition, T2-weighted interactive decomposition of water and fat with echo asymmetry least-squares estimation e Diffusion weighted imaging acquisition sequences.

RISULTATI: Nella valutazione delle strutture anatomiche contenute all'interno del canale mandibolare e della loro relazione spaziale con una lesione proliferativa della mandibola, la risonanza magnetica ha fornito informazioni spaziali e strutturali più dettagliate rispetto ai metodi di imaging tradizionali.

CONCLUSIONE: Le sequenze di acquisizione descritte hanno permesso di evidenziare l'efficacia diagnostica della risonanza magnetica nella caratterizzazione morfo-strutturale di una lesione maxillo-facciale e dei rapporti che essa contrae con il nervo alveolare inferiore, rendendo questa metodica un supplemento fondamentale alla tomografia computerizzata al fine di una corretta pianificazione chirurgica, con conseguente riduzione del rischio di lesione iatrogena del nervo alveolare inferiore.

References

- Barnes L, Eveson JW, Reichart P, Sidransky D: *World Health Organization classification of tumours: Pathology and genetics of head and neck tumours*. Lyon: International Agency for Research on Cancer Press, 2005.
- Cassetta M, Tarantino F, Calasso S: *Conservative treatment of odontogenic keratocyst: A case report and review of the literature*. Dental Cadmos, 2009; 77(7):19-40.
- Seo K, Terumistu M, Tanaka Y, Tsurumaki T, Kurata S, Matsuzawa H Takagi R: *Preoperative evaluation of spatial relationship between inferior alveolar nerve and Fibro-osseous lesion by high resolution magnetic resonance neurography on 3.0-T system: A case report*. J Oral Maxillofac Surg, 2012; 70:119-23.
- Cassetta M, Dell'Aquila D, Vozzolo SV, Bollero R: *Computer-aided implant therapy*. Dental Cadmos, 2007; 75(6):1-39.
- Cassetta M, Dell'Aquila D, Dolci A: *Healing times after bone graft*. Dental Cadmos, 2008; 76(1):27-36.
- Filler AG, Howe FA, Hayes CE, Kliot M, Winn HR, Bell BA, Griffiths JR, Tsuruda JS: *Magnetic resonance neurography*. Lancet, 1993; 341:659-61.
- Cassetta M, Dell'Aquila D, Dolci A: *Reconstruction of atrophic alveolar ridge*. Dental Cadmos, 2008; 76(6): 17-27.
- Cassetta M, Tarantino F, Calasso S: *CAD-CAM systems in titanium customized abutment construction*. Dental Cadmos, 2010; 78(4):27-44.
- Filler AG, Kliot M, Howe FA, Hayes CE, Saunders DE, Goodkin R, Bell BA, Winn HR, Griffiths JR, Tsuruda JS: *Application of magnetic resonance neurography in the evaluation of patients with peripheral nerve pathology*. J Neurosurg, 1996; 85:299-309.
- Cassetta M, Stefanelli LV, Giansanti M, Di Mambro A, Calasso S: *Depth deviation and occurrence of early surgical complications or unexpected events using a single stereolithographic surgi-guide*. Int J Oral Maxillofac Surg, 2011; 40:1377-87.
- Cassetta M, Di Mambro A, Giansanti M, Stefanelli LV, Cavallini C: *The intrinsic error of a stereolithographic surgical template in implant guided surgery*. Int J Oral Maxillofac Surg, 2013; 42(2):264-75. doi: 10.1016/j.ijom.2012.06.010. Epub 2012 Jul 11.
- Cassetta M, Giansanti M, Di Mambro A, Calasso S, Barbato E: *Accuracy of two stereolithographic surgical templates: A retrospective study*. Clin Implant Dent Relat Res. 2013; 15(3):448-59. doi: 10.1111/j.1708-8208.2011.00369.x. Epub 2011 Jul 11.
- Calasso S, Cassetta M, Galluccio G, Barbato E: *Impacted lower second molars*. Dental Cadmos; 76(2):41-54.
- Wei D, Song-Ling C, Zhong-Wei Z, Dai-Ying H, Xing Z, Xiang L: *High-resolution magnetic resonance imaging of the inferior alveolar nerve using 3-dimensional magnetization-prepared rapid gradient-echo sequence at 3.0T*. J Oral Maxillofac Surg, 2008; 66: 2621-626.
- Ikeda K, Ho KC, Nowicki BH, Haughton VM: *Multiplanar MR and anatomic study of the mandibular canal*. Am J Neuroradiol, 1996; 17:579-84.
- Nasel CJ, Pretterklieber M, Gahleitner A, Czerny C, Breitensteiner M, Imhof H: *Osteometry of the mandible performed using dental MR imaging*. Am J Neuroradiol, 1999; 20:1221-227.
- Eggers G, Rieker M, Fiebach J, Kress B, Dickhaus H, Hassfeld S: *Geometric accuracy of magnetic resonance imaging of the mandibular nerve*. Dentomaxillofac Radiol, 2005; 34:285-91.
- Mazza D, Marini M, Impara L, Cassetta M, Scarpato P, Barchetti F, Di Paolo C: *Anatomic examination of the upper head of the lateral pterygoid muscle using magnetic resonance imaging and clinical data*. J Craniofac Surg, 2009; 20:1508-511.
- Perrone A, Guerrisi P, Izzo L, D'Angeli I, Sassi S, Mele LL, Marini M, Mazza D, Marini M: *Diffusion-weighted MRI in cervical lymph nodes: Differentiation between benign and malignant lesions*. Eur J Radiol, 2011; 77:281-86.
- Rowley H, Grant E, Roberts T: *Diffusion MR imaging. Theory and application*. Neuroimaging Clin N Am, 1999; 9:343-61.
- Hisatomi M, Yanagi Y, Konouchi H, Matsuzaki H, Takenobu T, Unetsubo T, Asaumi J: *Diagnostic value of dynamic contrast-enhanced MRI for unilocular cystic-type ameloblastomas with homogeneously bright high signal intensity on T2-weighted or STI MR images*. Oral Oncol 2011; 47:147-52.
- Minami M, Kaneda T, Ozawa K, Yamamoto H, Itai Y, Ozawa M, Yoshikawa K, Sasaki Y: *Cystic lesions of the maxillomandibular region: MR imaging distinction of odontogenic keratocysts and ameloblastomas from other cysts*. Am J Roentgenol, 1996; 166:943-49.
- Hubáľková H, La Serna P, Linskij I, Dostálová T: *Dental alloys and magnetic resonance imaging*. Int Dent J, 2006; 56:135-41.
- Cassetta M, Di Carlo S, Pranno N, Stagnitti A, Pompa V, Pompa G: *The use of high resolution magnetic resonance on 3.0-T system in the diagnosis and surgical planning of intraosseous lesions of the jaws: Preliminary results of a retrospective study*. Eur Rev Med Pharmacol Sci. 2012; 16:2021-28.
- Cassetta M, Stefanelli LV, Di Carlo S, Pompa G, Barbato E: *The accuracy of CBCT in measuring jaws bone density*. Eur Rev Med Pharmacol Sci, 2012; 16:1425-29.